COBEM UBERLÂNDIA 2019

ABCM Associação Brasileira de Engenharia e Ciências Mecânicas

25th ABCM International Congress of Mechanical Engineering
October 20-25, 2019, Uberlândia, MG, Brazil

COB-2019-0786
DYNAMIC MODELING OF A PROSTHETIC KNEE

André Tura Markus
Rafael Antônio Comparsi Laranja
Mario Roland Sobczyk Sobrinho
Eduardo André Perondi
Universidade Federal do Rio Grande do Sul, Depto. Eng. Mecânica. Rua Sarmento Leite, 425, Porto Alegre-RS, Brasil
andre.markus@outlook.com, rafael.laranja@ufrgs.br, mario.sobczyk@ufrgs.br, eduardo.perondi@ufrgs.br

Abstract. *This work proposes a mathematical model of the dynamic behavior of prosthetic knees. The model is based on the biomechanics of actual human gait, employing multi-body dynamics tools for representing the studied system. The structure deformations due to contact forces are explicitly taken into account. Simulation results are used to illustrate the main features of the proposed model when compared to those obtained by means of a state-of-the-art commercial simulation package for mechanical systems. As result, the proposed algorithm and the commercial package have similar kinematic and dynamic behavior for free movement, while differ in the contact condition.*

Keywords: *knee prosthesis, multi-body dynamics, contact force, assistive technology*

1. INTRODUCTION

In order to develop a mechanism capable to restore locomotion a complete understating of human gait is mandatory. In bipedal walking, the gait is composed of two major phases: *stance*, when the foot is in contact with the ground, and *swing*, when the foot is suspended. During the swing phase, in a healthy person, a combination of movements reduce the total vertical length of the leg, allowing it to move freely without impact with the ground as the leg swings forward. After the point of lowest vertical distance, the leg extend, but maintain an constant angle of the knee in order to damp the incoming impact, as well as positioning the heel to be the first point of contact. The geometric characteristics of the mechanism representing the knee dictates the trajectory behavior of the leg, as well as the time it takes to complete its cycle. Currently commercially available prosthetic knees can be classified into two categories: a single axis knee and a polycentric knee. The first has a fixed axis of rotation and the position of the leg is controlled passively by one element which combines a damper and a spring. Its behavior is less than ideal, making it difficult for their users to control the movements performed by the leg and increasing the chance of intense, premature impacts (Rose and Gamble, 1998). As a result, amputees using low-quality prostheses are forced to move in a less "natural" fashion, pushing forward the thigh faster and higher and sweeping the lower limb sidewards to keep the prosthetic foot from crashing against the ground. As this sort of motion is very tiresome and uncomfortable, many amputees prefer to walk on crutches. Thus, whether they use prostheses or crutches, amputees become more likely to develop posture-related health issues in other body parts, such as hip and spine (Seymour, 2001). This is a matter of concern to the individual as well as to the public health care system, because the side-effects of such unnatural motions will lead the amputee to require further medical assistance from the government. As for a pure mechanical knee, the polycentric offers a better passive control, because it regulates the correct time of the movement during the swing phase and it locks the parts of the mechanism during the stance phase, allowing the transfer of the weight of its user to the prosthetic leg with safety and assurance (Rose and Gamble, 1998). Modern polycentric knees are composed of variations of linkage mechanisms with a spring-damper element. In an electronic controlled knee, the value of stiffness of the damper is variable and adjusted by a micro-controller. As for a mechanical knee, the stiffness of the damper and the pre-load of the spring are adjusted by the prothetist during the fitting of the prosthetic and in maintenance.

In recent academic works, there is an increase number of research of electronic prosthetic knees, for the benefit brought to the users gait by these prostheses, but this sophisticated technology also has a more expensive acquisition prices and even in development countries, they are often prohibitive for the majority of the population. One solution to this problem is the development of new designs for functional cost-effective mechanical prosthetic knees. A successful knee design depends on a number of factors, such as: the weight of the mechanism, its kinematic behavior, the mechanical resistance of its parts and the effect the prostheses has in the user center of gravity, to avoid excessive energy expenditure during multiple gait cycles. Many commercial computer-Aided Engineering (CAE) software provides packages for dynamic analysis of mechanisms, but they often have a cost of acquisition and demand a trained professional to operate and

analyses the results obtained.

In this work, we present an analysis of one prosthetic knee, using multi-body dynamic numerical method based on Principle of Virtual Work and Lagrangian dynamics. Additionally, we use a more complex method than the traditionally used by commercial software to calculate the impact force between its parts. This method is based on Herz Equation, and it is a very important feature because it allows accessing the impact absorption capabilities of the device. The chosen prosthetic knee model is a four-bar linkage mechanism often found in state-of-the art commercial prostheses. Although the method is applied to this particular mechanism, it can be reproduced to any other configuration. It also allows for the inclusion, within the same framework of equations, of more degrees of freedom as well as spring-damper devices and/or auxiliary actuators, so that more advanced mechanisms can be developed if required. Finally, the model also allows the computation of internal contact forces between its moving parts, been useful for its mechanical resistance assessment. The model is evaluated by means of simulation results based on experimental data, and its results are compared with commercial simulation package.

This work is organized as follows. In Section 2 the model is described, whereas its application is illustrated in Section 3. Finally, the main conclusions are outlined in Section 4.

2. MODEL DESCRIPTION

In this section, we describe the essential features of the proposed model, whose detailed derivation is presented in Markus (2015), which is written in Portuguese language. For a deep understanding from where the dynamic equations were obtained, the authors of this paper used the method described in Shabana (2010). The mechanism used in this analysis is illustrated in Figure 1, which presents a schematic view of complete prosthetic leg with a four-bar linkage knee, showing the centers of gravity of the rigid bodies that compose its structure, where Body #1 is composed of the Foot, Shank and an external housing, Body #2 is the anterior link, Body #3 is the combination of the leg and Socket and Body #4 the posterior link. The points **A**, **B**, **C** and **D** are rotational joints connecting each body and points **E** and **F** are rotational joints connecting Body #2 and #1 using a spring-damper element. The specific knee employed as the basis of the model was originally designed by Kramer *et al.* (1998), being depicted with its equivalent four-bar linkage mechanism in Fig. 2. This particular mechanism is a proposed evolution of one still available commercial knee. The author optimized the length of each link to obtain the most similar Instant Center of Rotation to a human counterpart. In Fig. 2 the blue part resembling a semicircle is a rubber cushion where contact forces occur between bodies #1 and #4, avoiding their impact during the use of the prosthesis.

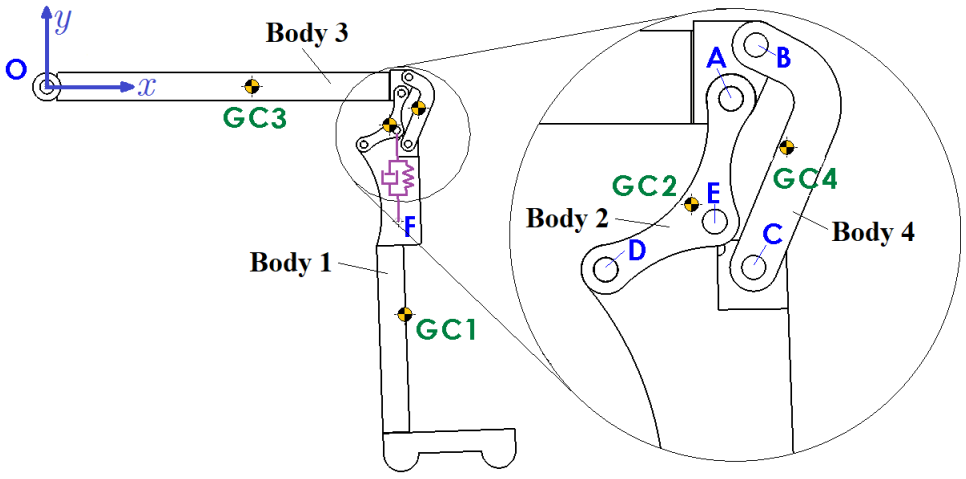

Figure 1: Schematic view of a prosthetic leg

All motion is restricted to the xy-plane, which is nearly true for a real knee (Shurr *et al.*, 2002). To specify the position (R_x, R_y) and orientation θ_i of each body, a local coordinate system its attach to the part respective gravity center. Thus, defining the generalized coordinates vector of each body as $\mathbf{q_i} = \begin{bmatrix} R_x^i & R_y^i & \theta^i \end{bmatrix}^T$, the instantaneous configuration of the system is

$$\mathbf{q} = [\mathbf{q}_1 \quad \mathbf{q}_2 \quad \dots \quad \mathbf{q}_{n_b}]^T \tag{1}$$

To model the system, the principle of virtual work its frequently used (Shabana, 2010), according to which, given a set $\mathbf{Q_e}$ of external generalized forces and torques acting upon the system, the generalized accelerations of its composing bodies satisfy

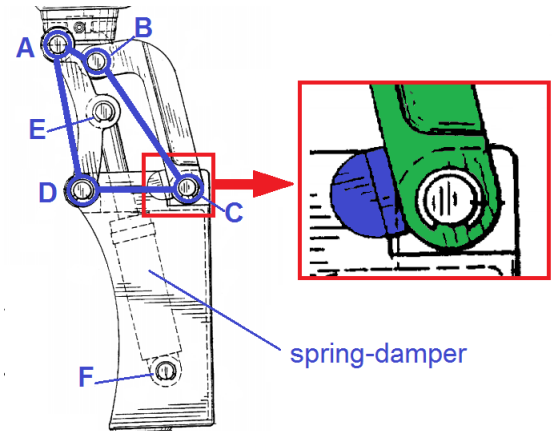

Figure 2: Prosthetic knee (adapted from Kramer *et al.* (1998))

$$\begin{bmatrix} \mathbf{M} & \mathbf{J}_\mathbf{q}^T \\ \mathbf{J}_\mathbf{q} & \mathbf{0} \end{bmatrix} \begin{bmatrix} \ddot{\mathbf{q}} \\ \boldsymbol{\lambda} \end{bmatrix} = \begin{bmatrix} \mathbf{Q}_e \\ \mathbf{Q}_d \end{bmatrix} \tag{2}$$

where $\mathbf{M}$ is the generalized mass matrix, $\mathbf{J}_\mathbf{q}$ is the Jacobian matrix, λ is the vector of Lagrange multipliers, and $\mathbf{Q}_d$ is the vector of *restriction equations*, which relate the positions, velocities and accelerations that are subject to geometric constraints, such as joint locations. Solving this equation for $\ddot{\mathbf{q}}$ results in the generalized accelerations of the bodies that compose the system, yielding the calculation of their corresponding velocities and displacements by numerical integration. This process is summarized in Fig. 3.

In order to facilitate its adoption with different geometric configurations and/or simulation platforms, the model presented here is basically analytical. However, due to their complexity, there are two parts of the algorithm whose analytical solution is very difficult to perform: (i) the determination of the geometric constraints $\mathbf{Q}_d$ employed in Eq. (2); (ii) calculation of the contact forces between bodies #1 and #4. In these two cases, calculation is carried out by means of numerical methods, as described in the following subsections.

2.1 Calculation of the geometric restrictions

Due to its geometric configuration, in order to solve the restriction equations for this system, it is necessary to deal with a large number of nonlinear trigonometric relations, which leads to the need of using numerical methods. In this work, the Newton-Raphson method is used, which is applied as follows. First, for a known configuration $\mathbf{q}$, all the geometric constraints of the system are written in a group of expressions $\mathbf{C}$, with their terms organized so as to ensure $\mathbf{C} = \mathbf{0}$. Then, to estimate the new configuration of the system as a result of a virtual displacement $\Delta\mathbf{q}$, it is expanded to the corresponding Taylor series:

$$\mathbf{C}(\mathbf{q} + \Delta\mathbf{q}, t) = \mathbf{C}(\mathbf{q}, t) + \mathbf{J}_\mathbf{q}\Delta\mathbf{q} + \frac{1}{2}\mathbf{J}_\mathbf{q}\left(\mathbf{J}_\mathbf{q}\Delta\mathbf{q}\right)\Delta\mathbf{q} + \ldots \tag{3}$$

Since the new configuration $\mathbf{q} + \Delta\mathbf{q}$ must also satisfy $\mathbf{C}(\mathbf{q} + \Delta\mathbf{q}, t) = \mathbf{0}$, by choosing a small $\Delta\mathbf{q}$ and neglecting the higher-order terms of the series it is obtained:

$$\mathbf{J}_\mathbf{q}\Delta\mathbf{q} = -\mathbf{C}(\mathbf{q}, t) \tag{4}$$

Thus, given an initial configuration $\mathbf{q}$, Eq. (4) is used to estimate the increment $\Delta\mathbf{q}$ that will take the system to a new valid configuration, i.e., to the new set of constraint relations to be employed in Eq. (2). Before this value is employed, its checked whether it is small enough to allow the truncation of the Taylor series using predictor-corrector Adams method. If it is too large, its set $\mathbf{q}_{k+1} = \mathbf{q}_k + \Delta\mathbf{q}_k$ and repeat the procedure until $||\Delta\mathbf{q}||$ is smaller than a desired limit.

2.2 Calculation of the contact forces

The modeling of the contact phenomena between rigid bodies is a topic in development (Machado *et al.*, 2012), (Lankarani and Nikravesh, 1990), (Zhiying and Qishao, 2006), (Hunt and Crossley, 1975), (Gonthier *et al.*, 2004), (Flores *et al.*, 2011). The main difficulty it is how to select the proper constitutive properties suited to describe the contact event,

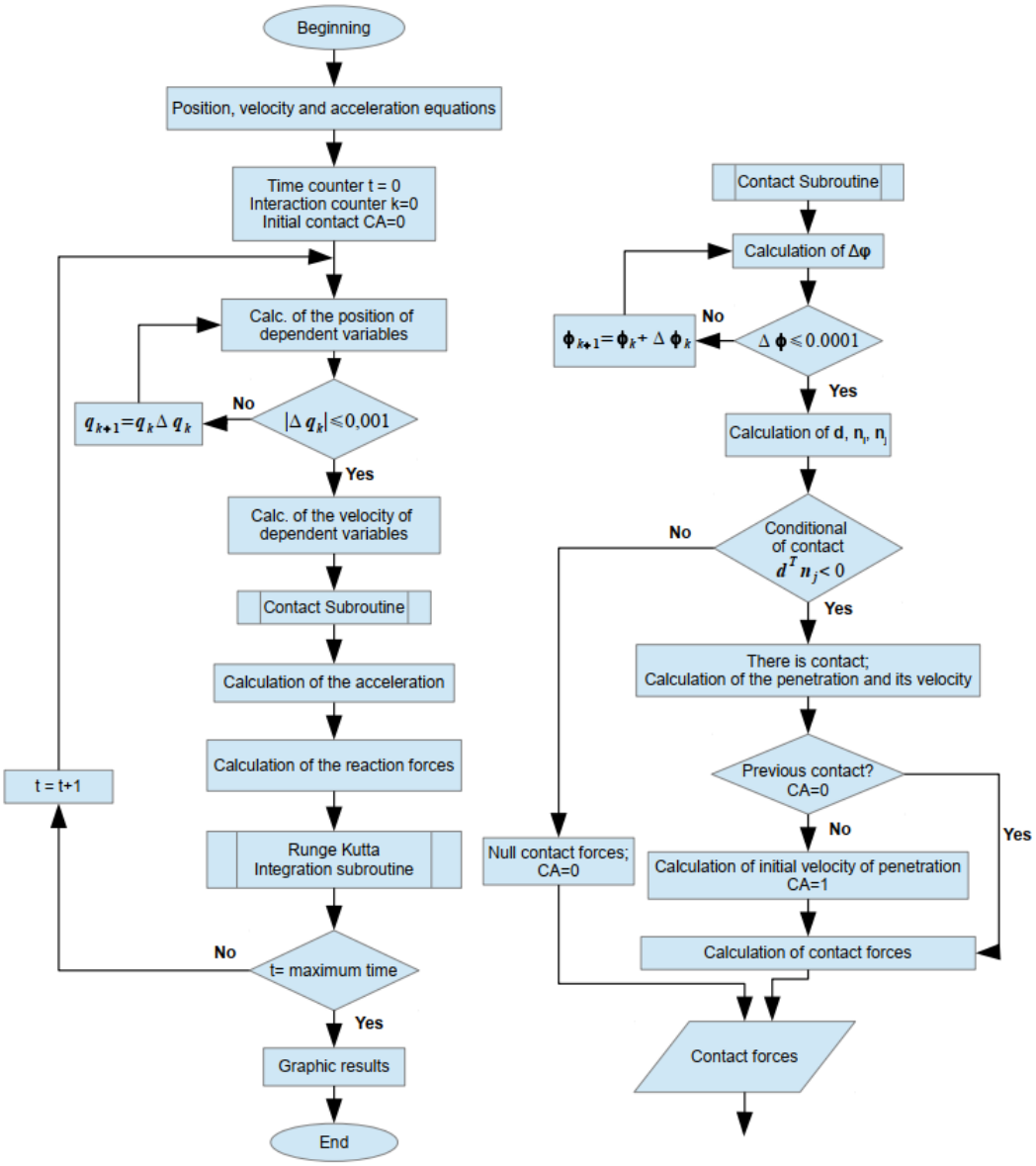

Figure 3: Proposed algorithm: main program and contact subroutine

due to the structural and geometric properties of the bodies in contact (Pham and Wang, 2011) (Ignacio Gonzalez-Perez, 2011) (Dopico *et al.*, 2010). Other parameters that are difficult to predict are the stiffness and the contact damping, as well as the dissipation of energy during the short time of the event.

The theoretical behavior of the contact of bodies in collision can be classified into two groups: i) *nonsmooth dynamics formulation* and ii) *regularized approach* (Flores, 2010). The first one is based on geometric restriction, where there is no deformation between the two rigid bodies, so there is no penetration from one body into another and the relative velocity is zero. This technique is efficient from a computational perspective, but it has difficulties associated to permanent contact and intermittent impact (Flores, 2010). In the second group, the bodies area allowed a local deformation in the point of contact, and the force generated is proportional to the relative penetration of the bodies (δ^n). The value of the contact force (F_N) can be calculated by different equations proposed by multiple authors. The most common is the Herz Equation, defined by:

$$F_N = K\delta^n \tag{5}$$

In Eq.(5) the value coefficient n depends on the form of distribution of the contact force and is usually determined empirically. The constant K depends on the geometry of the bodies and on its materials mechanical properties, such as Poisson Coefficient and Young Modulus (Machado *et al.*, 2012). This equation usually presents better results for elastic contacts, but even then, there is dissipation of energy involved. To incorporate this dissipative phenomena into the equation set, many authors proposed variations to Eq.(5). Goldsmith (1960) added a coefficient of restitution, where

resulting force depends on the relative velocity of the impact. Dubowsky *et al.* (1987) suggest that the components of the equations must be non-linear and proportional to the penetration and its velocity. Hunt and Crossley (1975) changed the dissipation component and added a non-linear one considering a hysteresis effect. In the work of Machado *et al.* (2012), the authors compared multiple analytical equations for assessment of contact force for a pre-defined body. A suitable result for a inelastic contact was performed by Flores *et al.* (2011), by means of Eq.6:

$$F_N = K\delta^n \left[1 + \frac{8(1-C_r)}{5C_r}\frac{\dot{\delta}}{\dot{\delta}^{(-)}}\right] \tag{6}$$

where K is the stiffness coefficient, C_r is the restitution coefficient, $\dot{\delta}$ is the penetration velocity between the two surfaces, and $\dot{\delta}_0$ is the value of such velocity at the instant when contact begins. In our algorithm, the contact force is based on this expression.

In current work, seeking to avoid eventual application misunderstandings with relation to the commercial softwares used for comparison of simulation results, we have opted not to mention them explicitly, referencing as CAE 1 and CAE 2, respectively.

The fist commercial software (CAE 1) apply a Penalty Method, due to its simplicity and computational efficiency. The Penalty approach for contact force is defined by Eq(7):

$$F_N = K\delta^n + STEP(\delta, 0, 0, d_{max}, c_{max})\dot{\delta} \tag{7}$$

Where *STEP* is a step function defined by:

$$STEP(a, x_1, y_1, x_2, y_2) = \begin{cases} y_1 & ; a \leq x_1 \\ y_1 + (x_2 - x_1)z^2(3-2z) & ; x1 < a < x_2 \\ y2 & ; a \geq x_2 \end{cases} \tag{8}$$

$$z = \frac{a - x_1}{x_2 - x_1} \tag{9}$$

Equations (8) and (9) are ruled by five parameters: I) a is the independent variable; II) x_1 is the value assumed by a when the function start to increase; III) y_1 is the value of the function before it reaches x_1; IV) x_2 the moment where the function stabilizes in a new reference value; V) y_2 the function value after stabilization. As an example, a function $STEP(time, 1, 1, 2, 2)$ has a value of 1 until 1 second, where it starts to increase defined by a cubic interpolation until it reaches a value of 2 at a time of 2 seconds and forward. In Eq.(7), $STEP$ has a value of zero when there is no penetration until a value of c_{max}, when the penetration is d_{max}.

The second software (CAE 2) uses a simple Coefficient of Restitution in order to calculate the velocity of both bodies after the contact, as a percentile of the velocity in the instant preceding the impact. As such, there is no penetration of parts and no local deformation, ignoring what really happens in this time period but only its consequence to the kinematic of the mechanism.

To be able to solve Eq.(6), one must know the relative penetration δ and its velocity $\dot{\delta}$, which consists in finding the minimum distance vector $\mathbf{d}$ between the surfaces of the two contacting bodies, whose description is parameterized as a function of their orientation angles φ_i and φ_j as illustrated in Fig. 4 (Machado *et al.*, 2010).

Based in the Fig.4, $\mathbf{R}^i$ is the position vector of the origin O_i of the local coordinate system of body i, expressed in the inertial reference system XY. The axis of the local system are $\xi_i\eta_i$ and θ_i is the angle of the local in respect to the global system. Been P_i a point located in the surface of body i where the maximum penetration occur, its local position vector is defined by $\mathbf{S}_i^P$, which has an angle of φ_i with the local ξ_i axis.

The surface which contains the point P_i belongs to body #4 (color green in Fig.(2)). This surface is represented by a polynomial S_i of third degree between the points A_i and B_i and can be written in polar coordinate φ_i as in the following equation:

$$S_i = a_3{\varphi_i}^3 + a_2{\varphi_i}^2 + a_1{\varphi_i}^1 + a_0 \tag{10}$$

where $a_{0,}a_1, a_2, a_3$ are cubic interpolation coefficients. The contact occurs between the surface of the body #4 and a 6 mm sphere attached to the frame of body #1, representing the blue part of Fig.(2). Both surfaces were expressed using known sphere and line equations in a polar coordinate system. The penetration of the bodies i and j is monitored by the position vector $\mathbf{d}$, which is the minimum distance between the two surfaces. Its value can be found by solving a system of three equations defined by Machado *et al.* (2010) and Flores (2010) as:

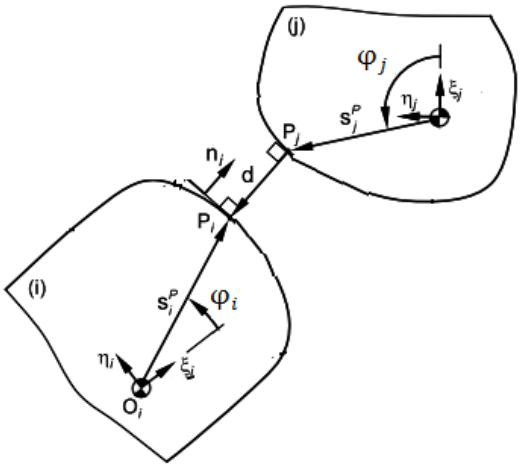

Figure 4: Basic framework for calculating contact forces (adapted from Machado *et al.* (2010))

$$\begin{cases} \mathbf{n}_j \times \mathbf{n}_i = \mathbf{0} \\ \mathbf{d} \times \mathbf{n}_i = \mathbf{0} \\ \mathbf{d} = \mathbf{r}_i^P - \mathbf{r}_j^P = \mathbf{R}^i + \mathbf{A}^i \mathbf{S}_i^P - \mathbf{R}^j - \mathbf{A}^j \mathbf{S}_j^P \end{cases} \tag{11}$$

Where $\mathbf{A^i}$ is the transformation matrix from the local to the inertial system, $\mathbf{S}_i^P$ the position vector of the surface, defined by Eq.(10). The first and second equations dictates that both vectors are normal to the surfaces and are collinear, as well as $\mathbf{d}$ is collinear to $\mathbf{n}_i$. The third equation ensures that the minimum distance between P_i and P_j is given by $\mathbf{d}$. To find a solution for $\mathbf{d}$, all the expressions must be functions of φ_i and φ_j. Eq.(11) can also be solved using dot product in the form:

$$\begin{cases} \mathbf{n}^{jT} \mathbf{t}_i = 0 \\ \mathbf{d}^T \mathbf{t}_i = 0 \end{cases} \qquad \mathbf{t}_i = \mathbf{A}^i \begin{bmatrix} \frac{d\xi_i^P}{d\varphi_i} & \frac{d\eta_i^P}{d\varphi_i} \end{bmatrix}^T \tag{12}$$

Eq.(12) is non-linear and to find the value for $\mathbf{d}$, φ_i and φ_j, the Newton-Raphson method for integration was used, leading to:

$$\mathbf{U} = \begin{bmatrix} \mathbf{n}^{jT} \mathbf{t}_i \\ \mathbf{d}^T \mathbf{t}_i \end{bmatrix} \qquad \mathbf{U}_{\varphi_i \varphi_j} \Delta\varphi = -\mathbf{U} \tag{13}$$

Where $\mathbf{U}_{\varphi_i \varphi_j}$ is the Jacobian of $\mathbf{U}$ in function of φ_i and φ_j and $\Delta\boldsymbol{\varphi}$ is the vector for Newton differences for the vector $\boldsymbol{\varphi} = [\varphi_i \quad \varphi_j]^T$. The penetration of one body into another happens when $\mathbf{d}^T \mathbf{n}_j < 0$ and its value is:

$$\delta = \sqrt{\mathbf{d}^T \mathbf{d}} \tag{14}$$

And the velocity of the penetration is:

$$\dot{\delta} = (\dot{\mathbf{r}}_i^P - \dot{\mathbf{r}}_j^P)^T \mathbf{n}_j \tag{15}$$

$$\dot{\mathbf{r}}_k^P = \dot{\mathbf{r}}_k + \dot{\mathbf{A}}^k \mathbf{S}_k^P \qquad (k = i, j) \tag{16}$$

$$\dot{\mathbf{r}}_k^P = \dot{\mathbf{r}}_k + \boldsymbol{\omega}^k \times \mathbf{A}_\theta^k \mathbf{S}_k^P \qquad (k = i, j) \tag{17}$$

$$\mathbf{A}_\theta^i = \frac{\partial \mathbf{A}}{\partial \theta^i} = \begin{bmatrix} -\sin\theta^i & -\cos\theta^i \\ cos\theta^i & -\sin\theta^i \end{bmatrix} \tag{18}$$

Where ω^k is the angular velocity of the body. When there is no penetration, the contact force is null. Otherwise, the force will be as in Eq.(6).

For comparison, the same system was modeled and simulated with the two commercial softwares. As much as possible, the parameter sets for all models were kept the same, using Aluminium 1060 as the material for thicker parts and Steel AISI 1010 for the parts with less thickness, such as body # 4 and the sphere of body # 1. Despite the original concept of sphere of Body # 1 been of rubber, the additional difficulty to model such material led to a momentary decision to simplify it and treat the material as AISI 1010 as well. In the material properties library of the CAE 1, the suggested values for the Stiffness Coefficient K, the maximum penetration d_{max} and maximum damping coefficient c_{max} were, respectively, $99.99x10^6 N/m$, $0.0001m$ and $49915.668 Nm/s$. In the same library, the Coefficient of Restitution C_r was 0.15. This value was used in both CAE 2 and in Eq.6 of the algorithm. By suggestion of Machado *et al.* (2012), the exponent n of Eq.6 used was 1.5. It is important to highlight that this last value is influenced by the geometry of the contact points.

The Table 1 presents the mass of each body.

Table 1: Values of Mass and Moment of Inertia for each body

Body	**1**	**2**	**3**	**4**
[$\mathbf{m_b}$ Kg]	1,774	0,225	2,144	0,196
[$\mathbf{J_b}$ MPa]	46702,61	210,69	61264,44	219,56

It was stipulated that the body starts each simulation with zero velocity and acceleration. The initial vector for generalized coordinates is presented in Table 2.

Table 2: Inicial vector for generalized global coordinates $\mathbf{q}$

R_x^1	R_y^1	θ^1
$-156,118 \times 10^{-3}$ m	$-830,897 \times 10^{-3}$ m	$5,87$ rad
R_x^2	R_y^2	θ^2
$-79,779 \times 10^{-3}$ m	$-549,955 \times 10^{-3}$ m	$5,72$ rad
R_x^3	R_y^3	θ^3
$-36,798 \times 10^{-3}$ m	$-291,284 \times 10^{-3}$ m	$6,16$ rad
R_x^4	R_y^4	θ^4
$-37,928 \times 10^{-3}$ m	$-559,137 \times 10^{-3}$ m	$5,67$ rad

Lastly, the local position vector for each joint of the four-bar linkage is:

$$\text{Body 1} \begin{cases} \overline{\mathbf{u}}_D^1 = \begin{bmatrix} -54,685 & 243,71 \end{bmatrix}^T 10^{-3} \quad \text{m} \\ \overline{\mathbf{u}}_C^1 = \begin{bmatrix} 8,815 & 243,759 \end{bmatrix}^T 10^{-3} \quad \text{m} \\ \overline{\mathbf{u}}_F^1 = \begin{bmatrix} -7,035 & -225,831 \end{bmatrix}^T 10^{-3} \quad \text{m} \end{cases} \qquad \text{Body 2} \begin{cases} \overline{\mathbf{u}}_A^2 = \begin{bmatrix} -20,538 & 43,792 \end{bmatrix}^T 10^{-3} \quad \text{m} \\ \overline{\mathbf{u}}_D^2 = \begin{bmatrix} -5,854 & -45,818 \end{bmatrix}^T 10^{-3} \quad \text{m} \\ \overline{\mathbf{u}}_E^2 = \begin{bmatrix} 12,205 & 1,99 \end{bmatrix}^T 10^{-3} \quad \text{m} \end{cases} \tag{19}$$

$$\text{Body 3} \begin{cases} \overline{\mathbf{u}}_A^3 = \begin{bmatrix} -9,804 & -213,667 \end{bmatrix}^T 10^{-3} \quad \text{m} \\ \overline{\mathbf{u}}_B^3 = \begin{bmatrix} 13,217 & -224,401 \end{bmatrix}^T 10^{-3} \quad \text{m} \\ \overline{\mathbf{u}}_E^3 = \begin{bmatrix} -0,521 & 293,599 \end{bmatrix}^T 10^{-3} \quad \text{m} \end{cases} \qquad \text{Body 4} \begin{cases} \overline{\mathbf{u}}_B^4 = \begin{bmatrix} -36,809 & 27,369 \end{bmatrix}^T 10^{-3} \quad \text{m} \\ \overline{\mathbf{u}}_C^4 = \begin{bmatrix} 19,118 & -49,733 \end{bmatrix}^T 10^{-3} \quad \text{m} \end{cases} \tag{20}$$

Where the letters follows the indications of Fig.(2).

The relative length of the damper-spring element is monitored. The force generated by the spring is proportional to its instant length, a unit position vector connecting bodies #1 and #2, at the points of attachment of the damper-spring element multiplied by its stiffness ($250 kN/m$). Thus, the representation of this vector, its modulus and the normalized vector are given by Eq.(21).

$$\mathbf{r}_P^{1,2} = \begin{bmatrix} \mathbf{R1} + \mathbf{A}^1 \mathbf{u}_F^1 - \mathbf{R2} + \mathbf{A}^2 \mathbf{u}_E^2 \end{bmatrix}^T \qquad l_{1,2} = \sqrt{\mathbf{r}_P^{1,2^T} \mathbf{r}_P^{1,2}} \qquad \mathbf{V} = \frac{\mathbf{r}_P^{1,2}}{L_{1,2}} \tag{21}$$

Where its generalized positions are:

$$\mathbf{q}_{1,2} = \begin{bmatrix} R_x^1 & R_y^1 & \theta^1 & R_x^2 & R_y^2 & \theta^2 \end{bmatrix}^T \qquad \dot{\mathbf{q}}_{1,2} = \begin{bmatrix} \dot{R}_x^1 & \dot{R}_y^1 & \dot{\theta}^1 & \dot{R}_x^2 & \dot{R}_y^2 & \dot{\theta}^2 \end{bmatrix}^T \tag{22}$$

The damping is proportional by the instant rate of its length change in respect to time, and is described by Eq.(23), multiplied by the its stiffness ($50kN.s/m$).

$$\dot{l}_{1,2} = \mathbf{V}^T \frac{\partial \mathbf{r}_{1,2}}{\partial \mathbf{q_{1,2}}} \dot{\mathbf{q}}_{1,2} \tag{23}$$

The resulting force is applied to the center of gravity of body #1 and #2 as an external force using an equipollent force system and its value is given by Eq.(24).

$$f_s = 250 \times 10^3 (l_{1,2} - l_0) + 50 \times 10^3 \dot{l}_{1,2} \tag{24}$$

More information about these formulation can be found in Shabana (2010) and Markus (2015).

In the simulations, it was applied a prescribed motion pattern to body #3, which represents the thigh, and the proposed model was processed in Matlab to predict the trajectories of the other three bodies in terms of angular position, velocity and acceleration, accompanied by the corresponding interaction forces. The input motion pattern was taken from a set of positions that represent the real motion of an individual during the stance phase of a standard gait test. Such data were acquired in videogammetry tests performed by Winter (2009), whose results can be freely accessed in *http://tinyurl.com/kxjh7js*. The data was transformed into an equivalent polynomial as in Fig.(5).

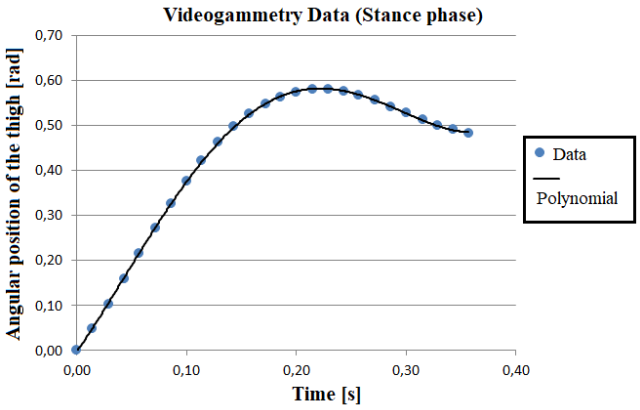

Figure 5: Videogammetry data use in prescribed motion of the thigh

3. SIMULATION RESULTS

The results from the simulations for body #1 are presented in Fig. (6). Since this body is the equivalent of the tube+foot assembly, its movements are the most representative of the usefulness of the model. The results pertaining to all other bodies can be found in Markus (2015). The thin dotted vertical lines in the graphs indicate the period during which the algorithm predicts contact forces.

The results indicate that, before contact occurs, the predictions given by the proposed model agree with those made by both commercial packages, with exception of results of CAE 2, where there is an excessive initial value for both velocity and acceleration, despite having the same starting values. This effect is probably due a small variation in initial length of the spring element. Once the contact is established, all the results differ. The algorithm have a rapid change in ratio of velocity and acceleration when compare to CAE 1, indicating a more inelastic behavior of the contact. This is more evident in Fig.6 (d), the proposed model responses reaching higher peaks and lasting for shorter periods. The CAE 2 does not register impact forces, only calculating the resulting velocity before and after the event. Thus, its values are not displayed in the figure. The resulting maximum penetration between Bodies #1 and #4 given by the proposed formulation and by CAD 1 are, respectively, 0.49 mm and 0.57 mm. Analyzing the results obtained by both methods it is observed an agreement in the displacement results, but a great difference in magnitude of peak contact force. In a standard Brinell test, a 10 mm sphere made of hardened steel (450 HD) is compressed against the material surface with constant force (29420 N) and the diameter o resulting indentation is measured. Using steel AISI 1010 with 105 HD, an expected indentation of 5.57 mm should result in a penetration of 0.909 mm. In a qualitative comparison, the order of magnitude of the displacement results obtained by both methods are similar with the standard test, but also indicates a behavior expected from harder materials. Thus, further studies must be carried out about the material properties used in the model, including an experimental evaluation of the system, before the implementation of the stance phase of the gait, which depends significantly of contact forces with the ground.

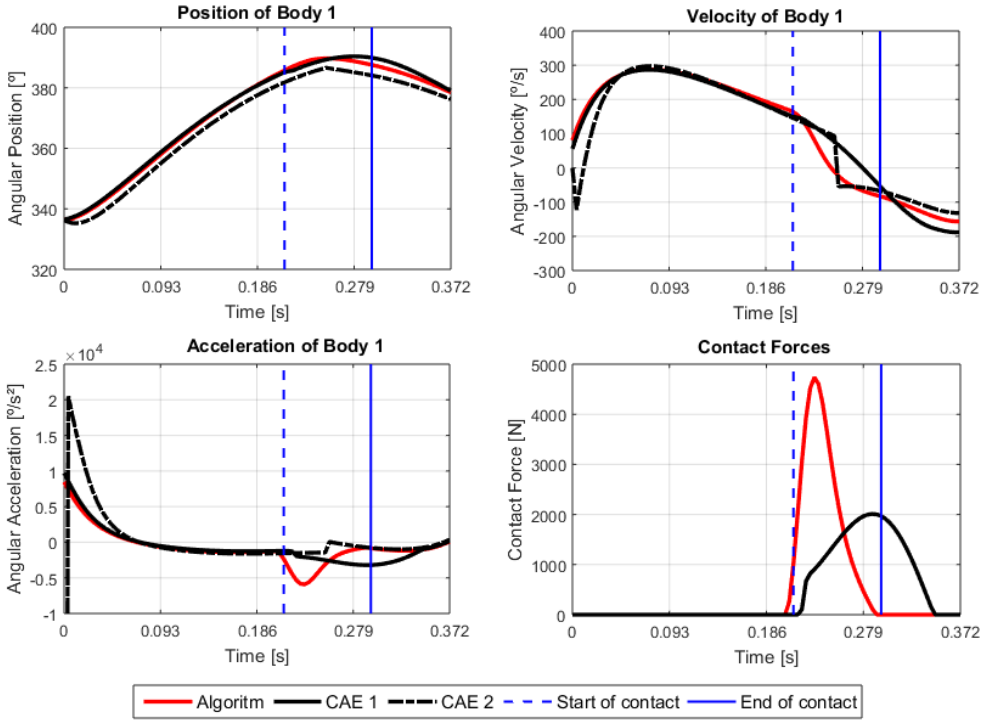

Figure 6: Simulation results: (a) angular position, (b) angular velocity, (c) angular velocity, (d) contact force

4. CONCLUSION

The proposed model is qualitatively consistent with the expected dynamic behavior of a polycentric knee prosthesis, and its results matches the ones found in popular commercial software. However, despite both methods to assess the contact force between rigid bodies had similar local deformation on the interacted bodies, the magnitude of calculated contact force differ. Before modeling the stance phase of the gait, a deeper analysis of the contact phenomena using experimental data must be executed. Further work will focus on the experimental validation of the model and the implementation of the stance phase.

5. ACKNOWLEDGEMENTS

This study was financed in part by the Coordenação de Aperfeiçoamento de Pessoal de Nível Superior – Brasil (CAPES).

6. REFERENCES

Dopico, D., Luaces, A., Gonzalez, M. and Cuadrado, J., 2010. "Dealing with multiple contacts in a human-in-the-loop application". *Multibody System Dynamics*, Vol. 25, No. 2, pp. 167–183. ISSN 1384-5640, 1573-272X. doi: 10.1007/s11044-010-9230-y. URL `http://link.springer.com/article/10.1007/s11044-010-9230-y`.

Dubowsky, S., Deck, J. and Costello, H., 1987. "The dynamic modeling of flexible spatial machine systems with clearance connections". *Journal of Mechanisms, Transmissions, and Automation in Design*, Vol. 109, pp. 87–94.

Flores, P., 2010. "A parametric study on the dynamic response of planar multibody systems with multiple clearance joints". *Nonlinear Dynamics*, Vol. 61, pp. 633–653.

Flores, P., Machado, M., Silva, M. and Martins, J., 2011. "On the continuous contact force models for soft materials in multibody dynamics". *Multibody System Dynamics*, Vol. 25, pp. 357–375.

Goldsmith, W., 1960. *Impact The Theory and Physical Behaviour of Colliding Solids*. Edward Arnold Ltd., London, England.

Gonthier, Y., McPhee, J., Lange, C. and Piedboeuf, J., 2004. "A regularized contact model with asymmetric damping and dwell-time dependent friction". *Multibody System Dynamics*, Vol. 11, pp. 209–233.

Hunt, K. and Crossley, F., 1975. "Coefficient of restitution interpreted as damping in vibroimpact". *Journal of Applied Mechanics*, Vol. 7, pp. 440–445.

Ignacio Gonzalez-Perez, J.L.I., 2011. "Implementation of hertz theory and validation of a finite element model for stress analysis of gear drives with localized bearing contact". *Mechanism and Machine Theory*, Vol. 46, No. 6. ISSN

0094-114X. doi:10.1016/j.mechmachtheory.2011.01.014.

Kramer, S., Srinivasan, S. and Swanson, V., 1998. "Knee joint mechanism for knee disarticulation prosthesis". URL `http://www.google.com.br/patents/US5746774`. U.S. Classification 623/39, 623/44; International Classification A61F2/64, A61F2/76, A61F2/74, A61F2/80, A61F2/50, A61F2/00; Cooperative Classification A61F2002/30507, A61F2/76, A61F2002/5016, A61F2/644, A61F2220/0025, A61F2002/745, A61F2/80; European Classification A61F2/76, A61F2/64P2.

Lankarani, H. and Nikravesh, P., 1990. "A contact force model with hysteresis damping for impact analysis of multibody systems". *Journal of Mechanical Design*, Vol. 112, pp. 369–376.

Machado, M., Flores, P., Claro, J., Ambrosio, J., Silva, M., Completo, A. and Lankarani, H., 2010. "Development of a planar multibody model of the human knee joint". *Nonlinear Dynamics*, Vol. 60, No. 3, pp. 459–478. ISSN 0924-090X, 1573-269X. doi:10.1007/s11071-009-9608-7.

Machado, M., Moreira, P., Flores, P. and Lankarani, H.L., 2012. "Compliant contact force models in multibody dynamics: Evolution of the hertz contact theory". *Mechanism and Machine Theory*, Vol. 53, pp. 99–121.

Markus, A.T., 2015. *Desenvolvimento de um algoritmo para um sistema dinâmico representante de um mecanismo de prótese de joelho*. Master's thesis, Universidade Federal do Rio Grande do Sul.

Pham, H.T. and Wang, D.A., 2011. "A constant-force bistable mechanism for force regulation and overload protection". *Mechanism and Machine Theory*, Vol. 46, No. 7. ISSN 0094114X. doi:10.1016/j.mechmachtheory.2011.02.008.

Rose, J. and Gamble, J.G., 1998. *Marcha Humana*. Premier, segunda edition. ISBN 85-86067-03-2.

Seymour, R., 2001. *Prosthetics and Orthotics: Lower Limb and Spinal*. Lippincott Williams Wilkins, 1st edition.

Shabana, A.A., 2010. *Computational Dynamics, 3rd Edition*. Wiley, Chichester, West Sussex ; Hoboken, 3rd edition. ISBN 9780470686157.

Shurr, D.G., Michael, J.W. and Cook, T.M., 2002. *Prosthetics and Orthotics*. Prentice Hall. ISBN 9780838581339.

Winter, D.A., 2009. *Biomechanics and Motor Control of Human Movement*. Wiley, Hoboken, N.J, 4th edition. ISBN 9780470398180.

Zhiying, Q. and Qishao, L., 2006. "Analysis of impact process based on restitution coefficien". *Journal of Dynamics and Control*, Vol. 4, pp. 294–298.

7. RESPONSIBILITY NOTICE

The authors are the only responsible for the printed material included in this paper.